Eur. Phys. J. Plus (2017) **132**: 517
DOI 10.1140/epjp/i2017-11803-3

THE EUROPEAN PHYSICAL JOURNAL PLUS

Regular Article

Impact of forced convective radiative heat and mass transfer mechanisms on 3D Carreau nanofluid: A numerical study

M. Khan, M. Irfan[a], and W.A. Khan

Department of Mathematics, Quaid-i-Azam University, Islamabad 44000, Pakistan

Received: 22 June 2017 / Revised: 7 October 2017
Published online: 12 December 2017 –

Abstract. Nanoliquids retain remarkable features that have fascinated various researchers owing to their utilization in nanoscience and nanotechnology. We will present a mathematical relation for 3D forced convective heat and mass transfer mechanism of a Carreau nanoliquid over a bidirectional stretched surface. Additionally, the features of heat source/sink and nonlinear thermal radiation are considered for the 3D Carreau nanoliquid. The governing nonlinear PDEs are established and altered into a set of nonlinear ODEs by utilizing a suitable conversion. A numerical approach, namely the bvp4c is adopted to resolve the resultant equations. The achieved outcomes are schemed and conferred in detail for somatic parameters. It is realized that amassed values of Brownian motion parameter N_b lead to enhance the temperature of the Carreau nanoliquid while quite conflicting behavior is being noticed for the concentration of the Carreau nanoliquid. Moreover, it is also noted that the influence of heat source $\delta > 0$ is relatively antithetic to heat sink $\delta < 0$ parameter, whereas an analogous impact is being identified for thermal Biot number γ on temperature and concentration Biot number γ_1 on concentration of the Carreau nanoliquid for shear thinning/thickening liquids. Additionally, an assessment between the analytical technique, namely the homotopy analysis method (HAM) and the numerical scheme bvp4c is presented graphically, as well as in tabular form. From these comparisons we initiate a splendid communication with these results.

1 Introduction

The latest technology-driven world enforces scientists and researchers to explore thermal engineering more and more. Presently, one of the most vital pursuits of thermal engineers is to provide efforts on new types of heat transfer liquids. They found that the addition of solid particles to a base liquid can provide the base liquid a better heat transfer capability. Additionally, based on this idea, a new generation liquid named as "nanoliquid" has arisen in the field for the last two decades. Although, this idea was first perceived by Choi [1]. Nanofluids are the diffusion of dense particles of magnitude lesser than 100 nm in liquids. Owing to the circumstance that dense particles present higher properties (directly correlated with heat transfer, *i.e.* thermal conductivities) than liquids. Nanofluids have progressively shown a better capacity of transferring thermal energy than their base fluids. Buongiorno [2] established a precise model to scrutinize the thermal assets of base liquids. He reported that the Brownian motion and thermophoresis enhance the thermal properties of base liquids. Afterwards, numerous researchers explored the stream of nanofluids under different situations and different sorts of nanoparticles. Analytically the entropy generation characteristics in MHD Cu–H2O nanoliquid was scrutinized by Ellahi *et al.* [3]. The impact of power law index in the existence of thermal radiation is occupied in this analysis. Numerical solutions for 3D magneto viscous nanofluids were established by Mahanthesh *et al.* [4]. Khan and Khan [5] investigated MHD power law nanofluid by utilizing the zero mass flux condition. A numerical scheme, namely the shooting technique was implemented to resolve the governing nonlinear ODEs. They pragmatically showed that both the Brownian motion and thermophoresis parameters were augmenting functions of the temperature distribution. Hayat *et al.* [6] analyzed numerically the stagnation point flow of a carbon-water nanofluid. The properties of melting heat and thermal energy were also deliberated in this exploration. They established that the amassed values of the melting parameter resemble to greater velocity and fewer temperature. Khan and Khan [7] considered the generalized Burgers nanoliquid with the influence of chemical response. The impact of nonlinear thermal radiation on the existence of the zero mass flux condition was also explored in this analysis.

[a] e-mail: mirfan@math.qau.edu.pk (corresponding author)

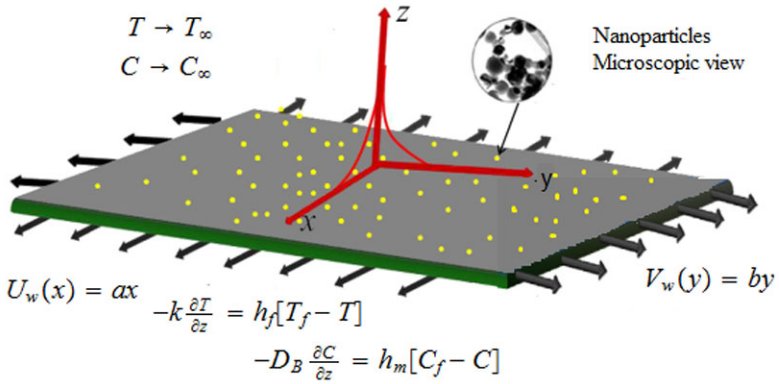

Fig. 1. Flow diagram.

The prose on the nanoliquids through diverse characteristics is substantial. Few latest endeavors around this region can be cited by the researchers (see refs. [8–15]) and numerous orientations therein.

The analysis of nonlinear difficulties dealing with the flow of non-Newtonian liquids has gained remarkable devotion during the former few decades. Such devotion is owing to their existence in oil reservoir manufacturing, geophysics, petroleum diligence, biochemical and nuclear-powered trades, polymer elucidation, synthetic fibers, cosmetic developments, etc. Undoubtedly, all non-Newtonian ingredients on the basis of their behavior in shear are not predicted by one constitutive relationship. Simple shear rate and stress terminologies cannot designate entirely the rheological structures of non-Newtonian fluids. Few endeavors in this trend can be accessed (see refs. [11,16–21]). Consequently, numerous constitutive terminologies for such fluids are suggested by the investigators in their scrutiny. Unlike, the power-law liquid model well-known as a Carreau viscosity model (generalized-Newtonian liquid model) whose constitutive manifestation is pertinent for the features of both shear thinning/thickening liquids. In 1972, Carreau [22] was the first who presented the rheological appearance of the Carreau liquid model. Afterwards, around numerous investigators considered the features of the Carreau liquid model in the flow substance to assorted characteristics. The flow of a Carreau liquid of blood through a tapered artery was analyzed by Akbar and Nadeem [23]. Hayat *et al.* [24] investigated analytically the Carreau nanoliquid in the existence of convective heat transport. They established that the velocity component rises for amassed values of the power law exponent.

Recently, owing to prominence in expertise and industrialized developments the flow analysis of convective heat transfer has extended a considerable concern amongst the investigators. It can play an enthusiastic amount in numerous manufacturing difficulties concerning both polymer and metallic sheets, high-performance biochemical catalysts, altercation of heat between functional heat storage beds and isolation of atomic vessels, etc. The notion of surface convective boundary condition was instigated by Aziz [25]. He deliberated the viscous fluid flow towards a flat plate with surface convective condition. The flow of an Eyring-Powell liquid with the combined impact of heat and mass convective condition was scrutinized by Hayat *et al.* [26]. They noted that the effects of thermal and mass Biot numbers on both the temperature and concentration was analogous. The solar energy and Joule heating influence in a thixotropic nanoliquid was considered by Hayat *et al.* [27]. The convective heat and mass transfer boundary condition is also taken into account in this exploration.

The above-mentioned scrutiny spectacles that flows with the simultaneous impact of convective heat and mass transport are not broadly considered. The current exploration intensifies the numerical investigation of the flow of a 3D Carreau nanofluid towards a bidirectional stretched surface. The heat transfer mechanism is conceded out under the influence of nonlinear thermal radiation and heat generation-absorption. Additionally, convective type boundary conditions on both the heat and mass transfer are occupied in this scrutiny. By invoking appropriate conversions the governing nonlinear PDEs are distorted into nonlinear ODEs and then resolved numerically by implementing the bvp4c scheme function in Matlab. The graphs are depicted and the table is organized for the temperature and the concentration field for various physical parameters and discussed in detail. Furthermore, an assessment between the numerical (bvp4c) and the analytical technique (HAM) are also presented graphically as well as in tabular form.

2 Problem formulation

We consider the steady 3D forced convective flow of a Carreau nanofluid over a bidirectional stretched surface. The effects of Brownian motion and thermophoresis particles are also occupied in this description. The flow is induced by stretching the surface in two adjacent x and y directions with linear velocity $u = ax$ and $v = by$, respectively, where a and b are positive constant and the fluid conquers the region $z > 0$ (as depicted in fig. 1). The heat transfer mechanism is conceded out in the presence of nonlinear thermal radiation and heat generation-absorption.

Under these norms with the standard boundary layer estimates, the existing flow problem of a Carreau nanofluid can be written as:

$$\frac{\partial u}{\partial x}+\frac{\partial v}{\partial y}+\frac{\partial w}{\partial z}=0, \tag{1}$$

$$u\frac{\partial u}{\partial x}+v\frac{\partial u}{\partial y}+w\frac{\partial u}{\partial z}=\nu\frac{\partial^2 u}{\partial z^2}\left[1+\Gamma^2\left(\frac{\partial u}{\partial z}\right)^2\right]^{\frac{n-1}{2}} + \nu(n-1)\Gamma^2\left(\frac{\partial u}{\partial z}\right)^2\frac{\partial^2 u}{\partial z^2}\left[1+\Gamma^2\left(\frac{\partial u}{\partial z}\right)^2\right]^{\frac{n-3}{2}}, \tag{2}$$

$$u\frac{\partial v}{\partial x}+v\frac{\partial v}{\partial y}+w\frac{\partial v}{\partial z}=\nu\frac{\partial^2 v}{\partial z^2}\left[1+\Gamma^2\left(\frac{\partial v}{\partial z}\right)^2\right]^{\frac{n-1}{2}} + \nu(n-1)\Gamma^2\left(\frac{\partial v}{\partial z}\right)^2\frac{\partial^2 v}{\partial z^2}\left[1+\Gamma^2\left(\frac{\partial v}{\partial z}\right)^2\right]^{\frac{n-3}{2}}, \tag{3}$$

$$u\frac{\partial T}{\partial x}+v\frac{\partial T}{\partial y}+w\frac{\partial T}{\partial z}=\alpha_1\frac{\partial^2 T}{\partial z^2}+\tau\left[D_B\frac{\partial C}{\partial z}\frac{\partial T}{\partial z}+\frac{D_T}{T_\infty}\left(\frac{\partial T}{\partial z}\right)^2\right] - \frac{1}{(\rho c)_f}\frac{\partial q_r}{\partial z}+\frac{Q_0}{(\rho c)_f}(T-T_\infty), \tag{4}$$

$$u\frac{\partial C}{\partial x}+v\frac{\partial C}{\partial y}+w\frac{\partial C}{\partial z}=D_B\frac{\partial^2 C}{\partial z^2}+\frac{D_T}{T_\infty}\frac{\partial^2 T}{\partial z^2}\,. \tag{5}$$

The flow problems subject to the resulting boundary conditions are

$$u=U_w(x)=ax,\qquad v=V_w(y)=by,\qquad w=0,$$

$$-k\frac{\partial T}{\partial z}=h_f[T_f-T]\quad -D_B\frac{\partial C}{\partial z}=h_m[C_f-C]\quad \text{at } z=0, \tag{6}$$

$$u\to 0,\quad v\to 0,\quad T\to T_\infty,\quad C\to C_\infty\quad \text{as } z\to\infty. \tag{7}$$

Here (u,v,w) are the velocity components in the x-, y- and z-directions, ν the kinematic viscosity, Γ the material rate constant, n the power law index, σ the electrical conductivity, (T,C) the temperature and volume friction of a nanoliquid, $\alpha_1(=\frac{k}{(\rho c)_f})$ the thermal diffusivity of a liquid, in which k is the thermal conductivity of a liquid, (ρ_f,c_f) the liquid density and specific heat, τ the ratio of effective heat capacity of nanoparticles to heat capacity of the base liquid, (D_B,D_T) the Brownian and thermal diffusion coefficients, respectively, q_r the radiative heat flux, (T_∞,C_∞) the ambient temperature and concentration of the nanoliquid, respectively, Q_0 the heat source/sink parameter. Moreover (h_f,h_m) are the wall heat and wall mass transfer coefficient, respectively, the convective heat mass transport is categorized by temperature and concentration (T_f,C_f) near to the surface, respectively.

For nonlinear thermal radiation, we utilize the Rosseland approximation, then the radiative heat flux q_r is simplified as

$$q_r=\frac{-16\sigma^* T_\infty^3}{3k^*}\frac{\partial T}{\partial z}\,, \tag{8}$$

in which (σ^*,k^*) are the Stefan-Boltzmann constant and mean absorption coefficient, respectively.

In view of an appropriate transformation

$$u=axf'(\eta),\qquad v=ayg'(\eta),\qquad w=-\sqrt{a\nu}[f(\eta)+g(\eta)],$$

$$\theta(\eta)=\frac{T-T_\infty}{T_f-T_\infty}\,,\qquad \phi=\frac{C-C_\infty}{C_f-C_\infty}\qquad \eta=z\sqrt{\frac{a}{\nu}}\,. \tag{9}$$

In the perception of overhead conversion, the condition of incompressibility is satisfied automatically and eqs. (2)–(9) reduced to

$$f'''\left[1+We_1^2 f''^2\right]^{\frac{n-3}{2}}\left[1+nWe_1^2 f''^2\right]-f'^2+f''(f+g)=0, \tag{10}$$

$$g'''\left[1+We_2^2 g''^2\right]^{\frac{n-3}{2}}\left[1+nWe_2^2 g''^2\right]-g'^2+g''(f+g)=0, \tag{11}$$

$$\frac{\mathrm{d}}{\mathrm{d}\eta}\left[\{1+R_d(1+(\theta_f-1)\theta)^3\}\theta'\right]+\Pr(f+g)\theta'+\Pr\left[N_b\theta'\phi'+N_t\theta'^2+\delta\theta\right]=0, \tag{12}$$

$$\phi''+\Pr Le(f+g)\phi'+\left(\frac{N_t}{N_b}\right)\theta''=0, \tag{13}$$

$$f(0)=0,\qquad g(0)=0,\qquad f'(0)=1,\qquad g'(0)=\alpha,$$

$$\theta'(0)=-\gamma(1-\theta(0))\qquad \phi'(0)=-\gamma_1(1-\phi(0)), \tag{14}$$

$$f'\to 0,\quad g'\to 0,\quad \theta\to 0\quad \phi\to 0\quad \text{as } \eta\to\infty. \tag{15}$$

In the above equations $We_1\left(=\sqrt{\frac{\Gamma^2 aU_w^2}{\nu}}\right)$ and $We_2\left(=\sqrt{\frac{\Gamma^2 aV_w^2}{\nu}}\right)$ are the local Weissenberg numbers, $R_d\left(=\frac{16\sigma^* T_\infty^3}{3kk^*}\right)$ the thermal radiation parameter, $N_b\left(=\frac{\tau D_B(C_f-C_\infty)}{\nu}\right)$ the Brownian motion parameter, $N_t\left(=\frac{\tau D_T(T_f-T_\infty)}{\nu T_\infty}\right)$ the thermophoresis parameter, $\Pr\left(=\frac{\nu}{\alpha_1}\right)$ the Prandtl number, $\delta\left(=\frac{Q_0}{a(\rho c)_f}\right)$ the heat source ($\delta>0$) and heat sink ($\delta<0$) parameter, $Le\left(=\frac{\alpha_1}{D_B}\right)$ the Lewis number, $\alpha\left(=\frac{b}{a}\right)$ the ratio of the stretching rates parameter, $\gamma\left(=\frac{h_f}{k}\sqrt{\frac{\nu}{\alpha}}\right)$ and $\gamma_1\left(=\frac{h_m}{D_B}\sqrt{\frac{\nu}{\alpha}}\right)$, are the thermal and concentration Biot numbers, respectively.

3 Engineering and industrial quantities of interest

From the industrial and engineering point of view, the essential quantities of physical interest are the skin friction, heat and transfer coefficients which may be defined by the subsequent expression:

$$C_{fx}=\frac{\tau_{xz}}{\frac{1}{2}\rho_f U_w^2},$$

$$C_{fy}=\frac{\tau_{yz}}{\frac{1}{2}\rho_f U_w^2}, \tag{16}$$

$$Nu_x=-\frac{x}{(T_f-T_\infty)}\left.\frac{\partial T}{\partial z}\right|_{z=0}+\frac{xq_r}{k(T_f-T_\infty)},$$

$$Sh_x=-\frac{x}{(C_f-C_\infty)}\left.\frac{\partial C}{\partial z}\right|_{z=0}. \tag{17}$$

The above quantity in the dimensionless forms:

$$\frac{1}{2}C_{fx}\,\mathrm{Re}_x^{\frac{1}{2}}=f''(0)\left[1+We_1^2 f''^2(0)\right]^{\frac{n-1}{2}},$$

$$\frac{1}{2}\left(\frac{U_w}{V_w}\right)C_{fy}\,\mathrm{Re}_x^{\frac{1}{2}}=g''(0)\left[1+We_2^2 g''^2(0)\right]^{\frac{n-1}{2}}, \tag{18}$$

$$\mathrm{Re}_x^{-\frac{1}{2}}\,Nu_x=-\left[1+R_d\{1+(\theta_f-1)\theta(0)\}^3\right]\theta'(0),$$

$$\mathrm{Re}_x^{-\frac{1}{2}}\,Sh_x=-\phi'(0), \tag{19}$$

in which $\mathrm{Re}_x=\frac{ax^2}{\nu}$ is the local Reynolds number.

4 Solution methodologies

4.1 Numerical scheme

The computation of the numerical scheme is established for nonlinear ODEs (10)–(13) with boundary conditions (14)-(15) via the bvp4c procedure [28–30]. To achieve this objective, we modify eqs. (10)–(15) into first order differential

structures are as follows:

$$f = y_1, \qquad f' = y_2, \qquad f'' = y_3, \qquad f''' = yy_1, \tag{20}$$

$$g = y_4, \qquad g' = y_5, \qquad g'' = y_6, \qquad g''' = yy_2, \tag{21}$$

$$\theta = y_7, \qquad \theta' = y_8, \qquad \theta'' = yy_3, \tag{22}$$

$$\phi = y_9, \qquad \phi' = y_{10}, \qquad \phi'' = yy_4, \tag{23}$$

$$yy_1 = \frac{-(y_1 + y_4)y_3 + y_2^2}{A_1}, \qquad A_1 = \left(1 + nWe_1^2 y_3^2\right) * \left(1 + We_1^2 y_3^2\right)^{\frac{n-3}{2}}, \tag{24}$$

$$yy_2 = \frac{-(y_1 + y_4)y_6 + y_5^2}{A_2}, \qquad A_2 = \left(1 + nWe_2^2 y_6^2\right) * \left(1 + We_2^2 y_6^2\right)^{\frac{n-3}{2}}, \tag{25}$$

$$yy_3 = \frac{-\Pr[(y_1 + y_4)y_8 + N_b y_8 y_{10} + N_t y_8^2 + \delta y_7] - 3R_d(1 + (\theta_f - 1)y_7)^2((\theta_f - 1)y_8^2)}{A_3} \tag{26}$$

$$A_3 = \left(1 + R_d(1 + (\theta_f - 1)y_7)^3\right), \tag{27}$$

$$yy_4 = -Le\Pr(y_1 + y_4) - \frac{N_t}{N_b} yy_3, \tag{28}$$

$$y_1(0) = 0, \qquad y_2(0) = 1, \qquad y_2(\infty) = 0, \tag{29}$$

$$y_4(0) = 0, \qquad y_5(0) = \alpha, \qquad y_5(\infty) = 0, \tag{30}$$

$$y_8(0) + \gamma(1 - y_7(0)) = 0, \qquad y_7(\infty) = 0, \tag{31}$$

$$y_{10}(0) + \gamma_1(1 - y_9(0)) = 0, \qquad y_9(\infty) = 0. \tag{32}$$

4.2 Homotopy analysis solutions (HAM)

The governing nonlinear ordinary differential eqs. (10)–(13) with boundary conditions (14) and (15) are solved by utilizing the homotopy analysis method (HAM) [31–33]. The initial guess $f_0(\eta)$, $g_0(\eta)$, $\theta_0(\eta)$ and $\phi_0(\eta)$ and the auxiliary linear operators $\mathcal{L}_f$, $\mathcal{L}_g$, $\mathcal{L}_\theta$ and $\mathcal{L}_\phi$ are chosen as follows:

$$\begin{aligned} f_0(\eta) &= 1 - \exp(-\eta), \\ g_0(\eta) &= \alpha\left[1 - \exp(-\eta)\right], \\ \theta_0(\eta) &= \frac{\gamma}{1+\gamma}\exp(-\eta), \\ \phi_0(\eta) &= \frac{\gamma_1}{1+\gamma_1}\exp(-\eta), \end{aligned} \tag{33}$$

$$\begin{aligned} \mathcal{L}_f[f(\eta)] &= \frac{\mathrm{d}^3 f}{\mathrm{d}\eta^3} - \frac{\mathrm{d}f}{\mathrm{d}\eta}, \\ \mathcal{L}_g[g(\eta)] &= \frac{\mathrm{d}^3 g}{\mathrm{d}\eta^3} - \frac{\mathrm{d}g}{\mathrm{d}\eta}, \\ \mathcal{L}_\theta[\theta(\eta)] &= \frac{\mathrm{d}^2\theta}{\mathrm{d}\eta^2} - \theta, \\ \mathcal{L}_\phi[\phi(\eta)] &= \frac{\mathrm{d}^2\phi}{\mathrm{d}\eta^2} - \phi, \end{aligned} \tag{34}$$

The above operators satisfying the following properties:

$$\mathcal{L}_f\left[C_1 + C_2\exp(\eta) + C_3\exp(-\eta)\right] = 0, \tag{35}$$

$$\mathcal{L}_g\left[C_4 + C_5\exp(\eta) + C_6\exp(-\eta)\right] = 0, \tag{36}$$

$$\mathcal{L}_\theta\left[C_7\exp(\eta) + C_8\exp(-\eta)\right] = 0, \tag{37}$$

$$\mathcal{L}_\phi\left[C_9\exp(\eta) + C_{10}\exp(-\eta)\right] = 0, \tag{38}$$

where $C_i (i = 1\text{–}10)$ are the arbitrary constants.

4.2.1 The zeroth-order deformation problems

The zeroth-order deformation problems are defined as follows:

$$(1-q)\mathcal{L}_f\left[\hat{f}(\eta,q)-f_0(\eta)\right]=q\hbar_f\mathcal{N}_f\left[\hat{f}(\eta,q),\hat{g}(\eta,q),\hat{\theta}(\eta,q),\hat{\phi}(\eta,q)\right], \tag{39}$$

$$(1-q)\mathcal{L}_g\left[\hat{g}(\eta,q)-g_0(\eta)\right]=q\hbar_g\mathcal{N}_g\left[\hat{f}(\eta,q),\hat{g}(\eta,q),\hat{\theta}(\eta,q),\hat{\phi}(\eta,q)\right], \tag{40}$$

$$(1-q)\mathcal{L}_\theta\left[\hat{\theta}(\eta,q)-\theta_0(\eta)\right]=q\hbar_\theta\mathcal{N}_\theta\left[\hat{f}(\eta,q),\hat{g}(\eta,q),\hat{\theta}(\eta,q),\hat{\phi}(\eta,q)\right], \tag{41}$$

$$(1-q)\mathcal{L}_\phi\left[\hat{\phi}(\eta,q)-\theta_0(\eta)\right]=q\hbar_\phi\mathcal{N}_\phi\left[\hat{f}(\eta,q),\hat{g}(\eta,q),\hat{\theta}(\eta,q),\hat{\phi}(\eta,q)\right], \tag{42}$$

$$\hat{f}(0,q)=0,\qquad \left.\frac{\partial\hat{f}(\eta,q)}{\partial\eta}\right|_{\eta=0}=1,\qquad \left.\frac{\partial\hat{f}(\eta,q)}{\partial\eta}\right|_{\eta\to\infty}=0, \tag{43}$$

$$\hat{g}(0,q)=0,\qquad \left.\frac{\partial\hat{g}(\eta,q)}{\partial\eta}\right|_{\eta=0}=\alpha,\qquad \left.\frac{\partial\hat{g}(\eta,q)}{\partial\eta}\right|_{\eta\to\infty}=0, \tag{44}$$

$$\hat{\theta}'(0,q)=-\gamma[1-\hat{\theta}(0,q)],\qquad \left.\hat{\theta}(\eta,q)\right|_{\eta\to\infty}=0, \tag{45}$$

$$\hat{\phi}'(0,q)=-\gamma_1[1-\hat{\phi}(0,q)],\qquad \left.\hat{\phi}(\eta,q)\right|_{\eta\to\infty}=0. \tag{46}$$

The nonlinear operators $\mathcal{N}_f$, $\mathcal{N}_g$, $\mathcal{N}_\theta$, and $\mathcal{N}_\phi$ are

$$\begin{aligned}\mathcal{N}_f\left[\hat{f}(\eta;q),\hat{g}(\eta;q),\hat{\theta}(\eta;q),\hat{\phi}(\eta;q)\right]&=\left(1+We_1^2\frac{\partial^2\hat{f}(\eta,q)}{\partial\eta^2}\right)^{\frac{n-3}{2}}\left(1+nWe_1^2\frac{\partial^2\hat{f}(\eta,q)}{\partial\eta^2}\right)\frac{\partial^3\hat{f}(\eta,q)}{\partial\eta^3}\\&\quad-\left(\frac{\partial\hat{f}(\eta,q)}{\partial\eta}\right)^2+\frac{\partial^2\hat{f}(\eta,q)}{\partial\eta^2}\left(\hat{f}+\hat{g}\right),\end{aligned} \tag{47}$$

$$\begin{aligned}\mathcal{N}_g\left[\hat{f}(\eta;q),\hat{g}(\eta;q),\hat{\theta}(\eta;q),\hat{\phi}(\eta;q)\right]&=\left(1+We_2^2\frac{\partial^2\hat{g}(\eta,q)}{\partial\eta^2}\right)^{\frac{n-3}{2}}\left(1+nWe_2^2\frac{\partial^2\hat{g}(\eta,q)}{\partial\eta^2}\right)\frac{\partial^3\hat{g}(\eta,q)}{\partial\eta^3}\\&\quad-\left(\frac{\partial\hat{g}(\eta,q)}{\partial\eta}\right)^2+\frac{\partial^2\hat{g}(\eta,q)}{\partial\eta^2}\left(\hat{f}+\hat{g}\right),\end{aligned} \tag{48}$$

$$\begin{aligned}\mathcal{N}_\theta\left[\hat{f}(\eta;q),\hat{g}(\eta;q),\hat{\theta}(\eta;q),\hat{\phi}(\eta;q)\right]&=\frac{\partial}{\partial\eta}\left[\left\{1+R_d\left(1+(\theta_f-1)\,\theta\right)^3\right\}\frac{\partial^2\hat{\theta}(\eta,q)}{\partial\eta^2}\right]\\&\quad+\Pr\left(\hat{f}+\hat{g}\right)\frac{\partial\hat{\theta}(\eta,q)}{\partial\eta}+\Pr N_b\frac{\partial\hat{\phi}(\eta,q)}{\partial\eta}\frac{\partial\hat{\theta}(\eta,q)}{\partial\eta}+\Pr N_t\left(\frac{\partial\hat{\theta}(\eta,q)}{\partial\eta}\right)^2+\Pr\delta\hat{\theta}(\eta,q),\end{aligned} \tag{49}$$

$$\mathcal{N}_\phi\left[\hat{f}(\eta;q),\hat{g}(\eta;q),\hat{\theta}(\eta;q),\hat{\phi}(\eta;q)\right]=\frac{\partial^2\hat{\phi}(\eta,q)}{\partial\eta^2}+\Pr Le\left(\hat{f}+\hat{g}\right)\frac{\partial\hat{\phi}(\eta,q)}{\partial\eta}+\left(\frac{N_t}{N_b}\right)\frac{\partial^2\hat{\theta}(\eta,q)}{\partial\eta^2}. \tag{50}$$

For $q=0$ and $q=1$, we have

$$\begin{aligned}&\hat{f}(\eta;0)=f_0(\eta),\qquad \hat{f}(\eta;1)=f(\eta),\\&\hat{g}(\eta;0)=g_0(\eta),\qquad \hat{g}(\eta;1)=g(\eta),\\&\hat{\theta}(\eta;0)=\theta_0(\eta),\qquad \hat{\theta}(\eta;1)=\theta(\eta),\\&\hat{\phi}(\eta;0)=\phi_0(\eta),\qquad \hat{\phi}(\eta;1)=\phi(\eta).\end{aligned} \tag{51}$$

Note that $f_0(\eta)$, $g_0(\eta)$, $\theta_0(\eta)$ and $\phi_0(\eta)$ approach $f(\eta)$, $g(\eta)$, $\theta(\eta)$ and $\phi(\eta)$, respectively, when q has variation from 0 to 1. According to the Taylor series we have

$$\hat{f}(\eta,q)=f_0(\eta)+\sum_{m=1}^{\infty}f_m(\eta)q^m,\qquad f_m(\eta)=\frac{1}{m!}\frac{\partial^m f(\eta,q)}{\partial q^m}\bigg|_{q=0}, \tag{52}$$

$$\hat{g}(\eta,q)=g_0(\eta)+\sum_{m=1}^{\infty}g_m(\eta)q^m,\qquad g_m(\eta)=\frac{1}{m!}\frac{\partial^m g(\eta,q)}{\partial q^m}\bigg|_{q=0}, \tag{53}$$

$$\hat{\theta}(\eta,q)=\theta_0(\eta)+\sum_{m=1}^{\infty}\theta_m(\eta)q^m,\qquad \theta_m(\eta)=\frac{1}{m!}\frac{\partial^m \theta(\eta,q)}{\partial q^m}\bigg|_{q=0}, \tag{54}$$

$$\hat{\phi}(\eta,q)=\phi_0(\eta)+\sum_{m=1}^{\infty}\phi_m(\eta)q^m,\qquad \phi_m(\eta)=\frac{1}{m!}\frac{\partial^m \phi(\eta,q)}{\partial q^m}\bigg|_{q=0}. \tag{55}$$

The values of $\hbar_f$, $\hbar_g$, $\hbar_\theta$ and $\hbar_\phi$ are chosen in such a way that the series (52)–(55) are convergent at $q=1$ and hence

$$f(\eta)=f_0(\eta)+\sum_{m=1}^{\infty}f_m(\eta), \tag{56}$$

$$g(\eta)=g_0(\eta)+\sum_{m=1}^{\infty}g_m(\eta), \tag{57}$$

$$\theta(\eta)=\theta_0(\eta)+\sum_{m=1}^{\infty}\theta_m(\eta), \tag{58}$$

$$\phi(\eta)=\phi_0(\eta)+\sum_{m=1}^{\infty}\phi_m(\eta). \tag{59}$$

4.2.2 The m-th order deformation problems

The m-th order deformation problems are of the form

$$\mathcal{L}_f\left[f_m(\eta)-\chi_m f_{m-1}(\eta)\right]=\hbar_f\mathcal{R}_m^f(\eta), \tag{60}$$

$$\mathcal{L}_g\left[g_m(\eta)-\chi_m g_{m-1}(\eta)\right]=\hbar_g\mathcal{R}_m^g(\eta), \tag{61}$$

$$\mathcal{L}_\theta\left[\theta_m(\eta)-\chi_m \theta_{m-1}(\eta)\right]=\hbar_\theta\mathcal{R}_m^\theta(\eta), \tag{62}$$

$$\mathcal{L}_\phi\left[\phi_m(\eta)-\chi_m \phi_{m-1}(\eta)\right]=\hbar_\phi\mathcal{R}_m^\phi(\eta), \tag{63}$$

$$\begin{aligned}
&f_m(0)=0,\qquad \frac{\partial f_m(\eta)}{\partial\eta}\bigg|_{\eta=0}=0,\qquad \frac{\partial f_m(\eta)}{\partial\eta}\bigg|_{\eta\to\infty}=0,\\
&g_m(0)=0,\qquad \frac{\partial g_m(\eta)}{\partial\eta}\bigg|_{\eta=0}=0,\qquad \frac{\partial g_m(\eta)}{\partial\eta}\bigg|_{\eta\to\infty}=0,\\
&\theta_m'(0)-\gamma\theta_m(0)=\theta_m(\infty)=0,\\
&\phi_m'(0)-\gamma_1\phi_m(0)=\phi_m(\infty)=0,
\end{aligned} \tag{64}$$

where

$$\chi_m=\begin{cases}0; & m\leqslant 1,\\ 1; & m>1.\end{cases} \tag{65}$$

$$\mathcal{R}_m^f(\eta)=-\sum_{k=0}^{m-1}f_{m-1-k}'f_k'+\sum_{k=0}^{m-1}f_{m-1-k}''(f_k+g_k)+\varphi_f(\eta), \tag{66}$$

$$\mathcal{R}_m^g(\eta)=-\sum_{k=0}^{m-1}g_{m-1-k}'g_k'+\sum_{k=0}^{m-1}g_{m-1-k}''(f_k+g_k)+\varphi_g(\eta), \tag{67}$$

$$\mathcal{R}_m^{\theta}(\eta) = (1+R_d)\theta''_{m-1}(\eta) + R_d\,(\theta_f-1)^3 \sum_{k=0}^{m-1}\theta_{m-1-k}\sum_{l=0}^{k}\theta_{k-l}\sum_{j=0}^{l}\theta_{l-j}\theta''_j + 3R_d\,(\theta_f-1)^2\sum_{k=0}^{m-1}\theta_{m-1-k}\sum_{l=0}^{k}\theta_{k-l}\theta''_l$$
$$+ 3R_d\,(\theta_f-1)\sum_{k=0}^{m-1}\theta_{m-1-k}\theta''_k + 3R_d\,(\theta_f-1)\sum_{k=0}^{m-1}\theta'_{m-1-k}\theta'_k + 6R_d\,(\theta_f-1)^2\sum_{k=0}^{m-1}\theta_{m-1-k}\sum_{l=0}^{k}\theta'_{k-l}\theta'_l$$
$$+ 3R_d\,(\theta_f-1)^3\sum_{k=0}^{m-1}\theta_{m-1-k}\sum_{l=0}^{k}\theta_{k-l}\sum_{j=0}^{l}\theta'_{l-j}\theta'_j + \Pr\sum_{k=0}^{m-1}(f_{m-1-k}+g_{m-1-k})\,\theta'_k$$
$$+ \Pr N_b\sum_{k=0}^{m-1}\theta'_{m-1-k}\phi'_k + \Pr N_t\sum_{k=0}^{m-1}\theta'_{m-1-k}\theta'_k + \Pr\delta\theta_{m-1}, \tag{68}$$

$$\mathcal{R}_m^{\phi}(\eta) = \phi''_{m-1}(\eta) + \left(\frac{N_t}{N_b}\right)\theta''_{m-1}(\eta) + \Pr Le\sum_{k=0}^{m-1}\phi'_{m-1-k}\,(f_k+g_k), \tag{69}$$

where

$$\varphi_f(\eta) = \begin{cases} = f'''_{m-1}, & n=1,\\ = f'''_{m-1} + 3We_1^2\sum_{k=0}^{m-1} f'''_{m-1-k}\sum_{l=0}^{k} f''_{k-l}f''_l, & n=3, \end{cases} \tag{70}$$

$$\varphi_g(\eta) = \begin{cases} = g'''_{m-1}, & n=1,\\ = g'''_{m-1} + 3We_2^2\sum_{k=0}^{m-1} g'''_{m-1-k}\sum_{l=0}^{k} g''_{k-l}g''_l, & n=3, \end{cases} \tag{71}$$

where the general solutions are

$$f_m(\eta) = f_m^*(\eta) + C_1 + C_2\exp(\eta) + C_3\exp(-\eta), \tag{72}$$
$$g_m(\eta) = g_m^*(\eta) + C_4 + C_5\exp(\eta) + C_6\exp(-\eta), \tag{73}$$
$$\theta_m(\eta) = \theta_m^*(\eta) + C_7\exp(\eta) + C_8\exp(-\eta), \tag{74}$$
$$\phi_m(\eta) = \phi_m^*(\eta) + C_9\exp(\eta) + C_{10}\exp(-\eta), \tag{75}$$

where f_m^*, g_m^*, θ_m^* and ϕ_m^* denote the particular solutions and the constants c_i (i = 1–10) can be determined by utilizing the boundary conditions. They are given by

$$c_3 = \left.\frac{\partial f^*(\eta)}{\partial\eta}\right|_{\eta=0}, \qquad c_1 = -c_3 - f^*(0), \qquad c_6 = \left.\frac{\partial g^*(\eta)}{\partial\eta}\right|_{\eta=0}, \qquad c_4 = -c_6 - g^*(0),$$
$$c_8 = \frac{1}{1+\gamma}\left[\left.\frac{\partial\theta^*(\eta)}{\partial\eta}\right|_{\eta=0} - \gamma\theta^*(0)\right], \qquad c_{10} = \frac{1}{1+\gamma_1}\left[\left.\frac{\partial\phi^*(\eta)}{\partial\eta}\right|_{\eta=0} - \gamma_1^*\phi(0)\right], \qquad c_2 = c_5 = c_7 = c_9 = 0. \tag{76}$$

5 Numerical results and discussion

This section is concentrated to analyze the influence of various physical parameters on the temperature and concentration of a Carreau nanoliquid, respectively. A set of combined nonlinear ODEs (10) to (13) with boundary conditions (14) and (15) are interpreted numerically by employing the bvp4v technique. Graphs are portrayed for the values of diverse flow parameters. Furthermore, the outcomes for the local Nusselt number and Sherwood number are tabularized and discuss in detail.

Figures 2(a), (b) and 3(a), (b) are portrayed to visualize the impact of the Brownian motion parameter and thermophoresis parameter on nanoliquid temperature for shear thinning/thickening liquids. From these plots it is detected that both parameters are an augmenting function of the temperature of the Carreau liquid for rising values of these parameters. Physically, the Brownian motion parameter, depends on the Brownian motion of nanoparticles in the Carreau liquid. As we augmented the Brownian motion parameter the random motion of the particles rises due to which the velocity of the nanoparticles boosts. Therefore, the temperature of the Carreau nanoliquid enhances. Moreover, the thermophoresis parameter is directly proportional to the difference of temperature between the wall and

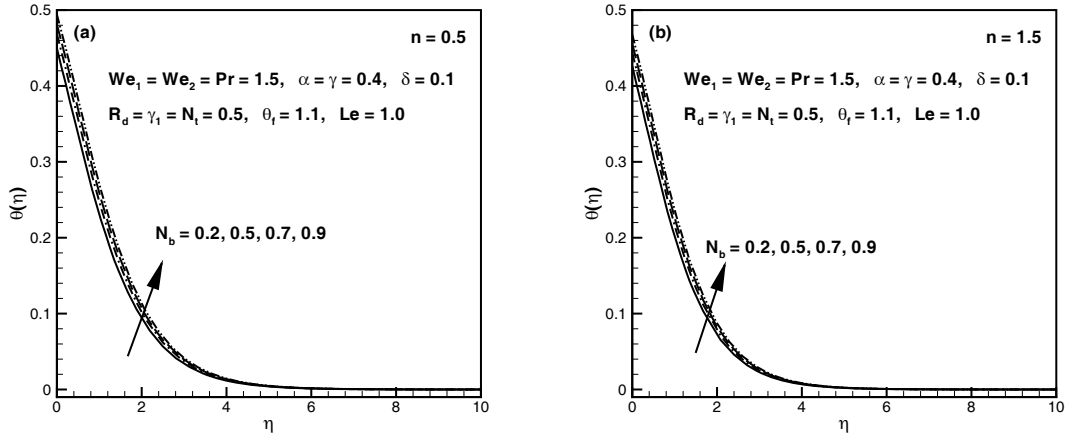

Fig. 2. Impact of Brownian motion parameter N_b on temperature field $\theta(\eta)$.

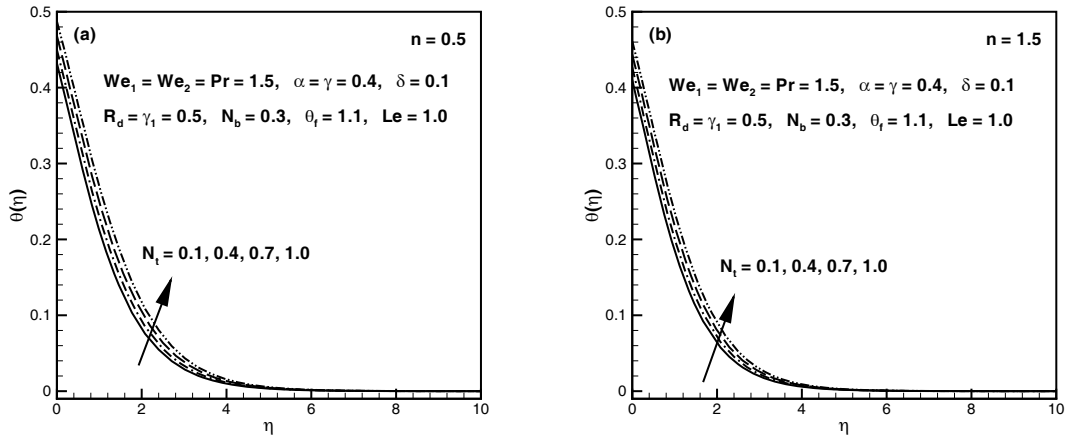

Fig. 3. Impact of thermophoresis parameter N_t on temperature field $\theta(\eta)$.

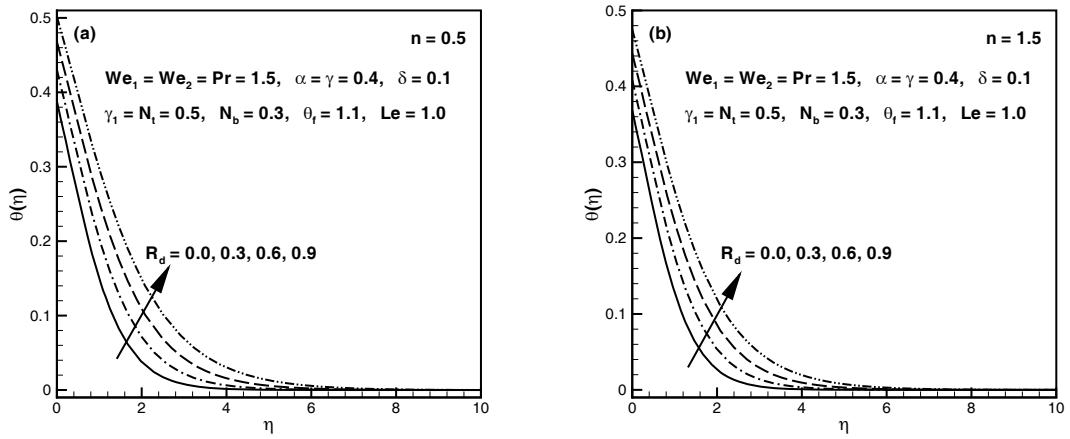

Fig. 4. Impact of radiation parameter R_d on temperature field $\theta(\eta)$.

the reference temperature. In the flow domain of the particulate structure, there is a temperature gradient in hotter regions which causes small inclined elements to isolate quicker. Consequently, the surface temperature of the nanoliquid and its thickness of boundary layer enhance. Additionally, growing the values of thermophoresis parameter physically means that the smallest nanoparticles are pulled away from the warm surface to the cold surface. Therefore, the higher number of small nanoparticles is dragged away from the warm surface due to which concentration of the nanoliquid declines. Figures 4(a), (b) and 5(a), (b) are plotted to determine the features of thermal radiation parameter R_d and temperature ratio parameter θ_f on the temperature distribution for shear thinning and shear thickening liquids.

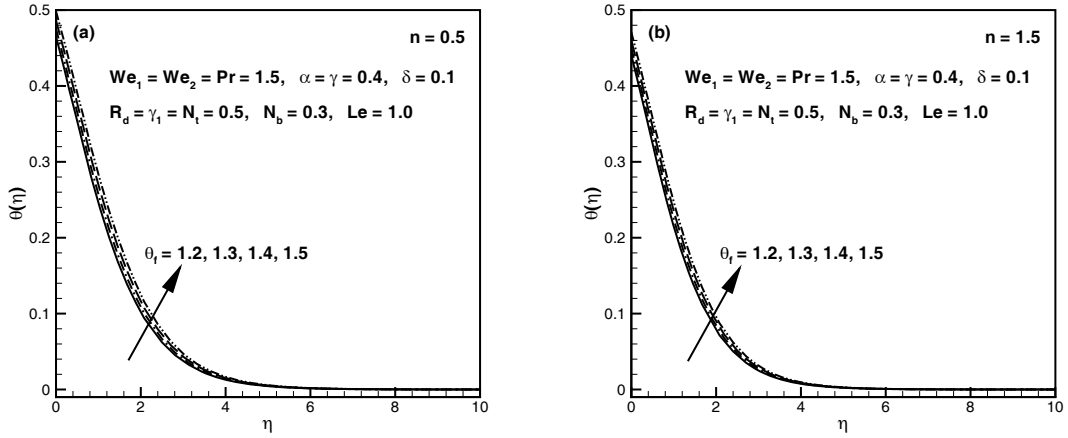

Fig. 5. Impact of temperature ratio parameter θ_f on temperature field $\theta(\eta)$.

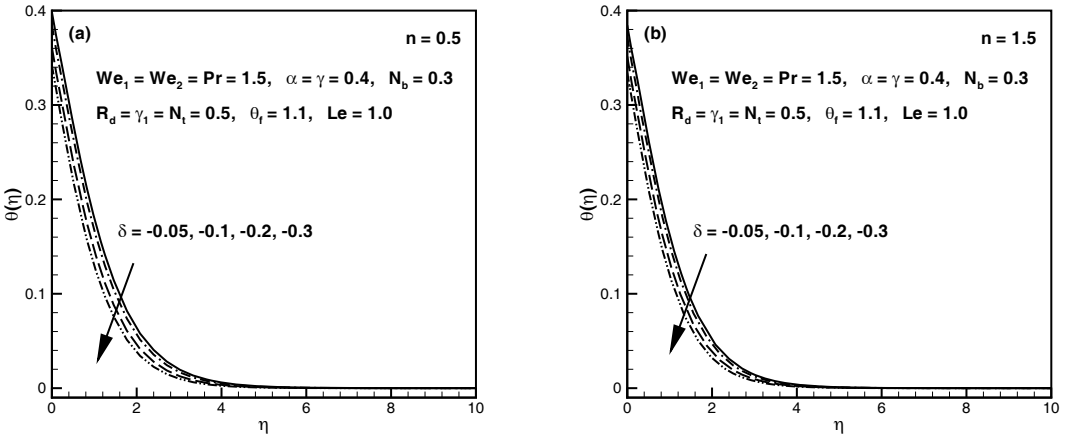

Fig. 6. Impact of heat sink parameter ($\delta < 0$) on temperature field $\theta(\eta)$.

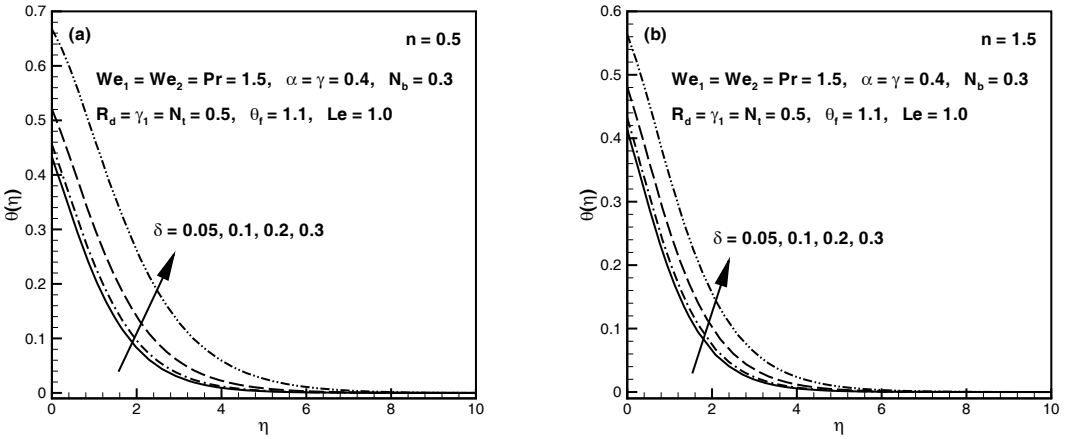

Fig. 7. Impact of heat source parameter ($\delta > 0$) on temperature field $\theta(\eta)$.

It is noted that the temperature and its related thickness of boundary layer enhance for the amassed values of these parameters in both instances. From the physical point of view increasing the values of the radiation parameter formed much heat in the working liquid which consequently augments the temperature distribution. Figures 6(a), (b) and 7(a), (b) clarified the properties of the heat absorption/generation parameter on the nanoparticles temperature field. From these sketches it is established that the temperature of the Carreau nanoliquid and associated thermal boundary layer thickness decline when we rise the values of the heat absorption parameter however the conflicting circumstance is being pragmatic for the heat generation parameter. Apparently the heat generation phenomenon

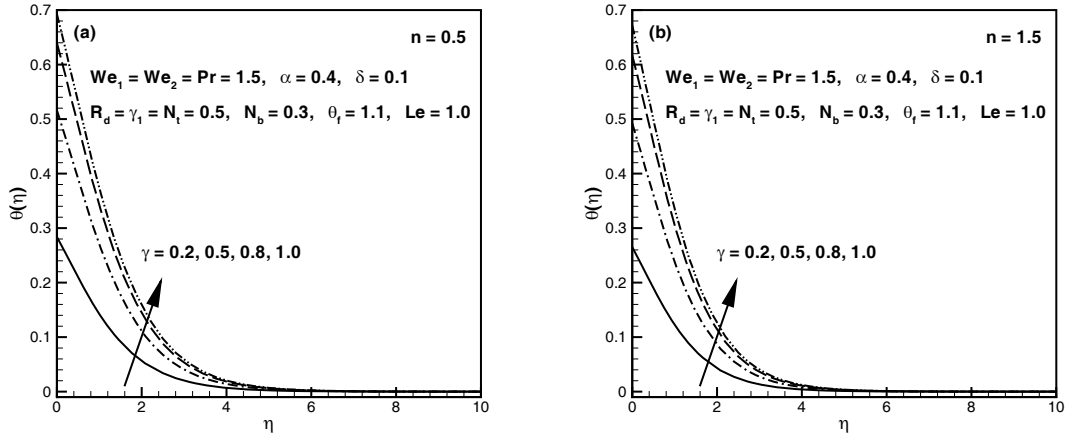

Fig. 8. Impact of thermal Biot number γ on temperature field $\theta(\eta)$.

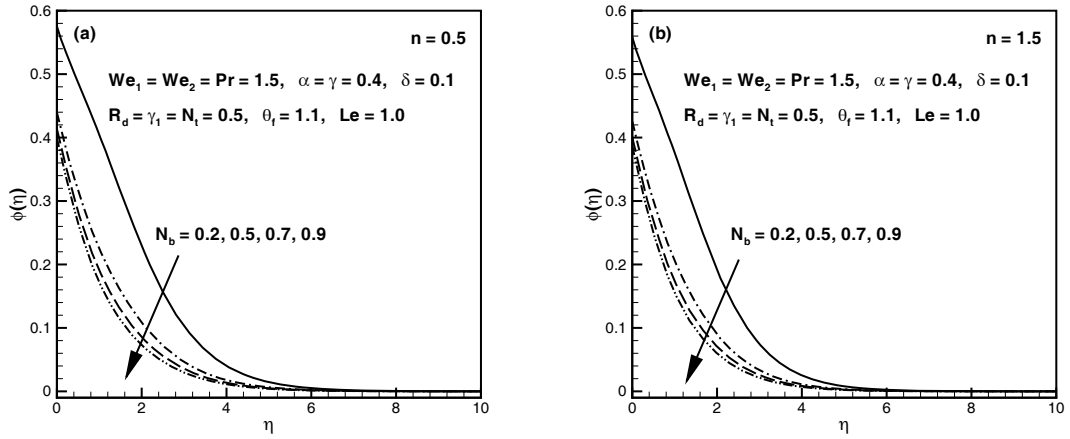

Fig. 9. Impact of Brownian motion parameter N_b on concentration field $\phi(\eta)$.

provides much heat to the liquid that corresponds to the increase in the temperature profile for both ($n < 1$) and ($n > 1$). The influence of increasing values of the thermal Biot number γ for shear thinning/thickening liquids on the temperature distribution is portrayed in fig. 8(a), (b). We can perceive from these designs that augmenting behavior for amassed values of γ on the temperature distribution is detected. As an increase in the thermal Biot number occurs the convection of the surface rises and as a result it enhances the liquid temperature and its allied thickness of the boundary layer.

Figures 9(a), (b) and 10(a), (b) are delineated to interpret the characteristics of the Brownian motion N_b and thermophoresis parameter N_t, respectively on the concentration of the nanoliquid. We can comprehend that the concentration of the Carreau nanoliquid and associated concentration boundary layer thickness diminish for the larger values of the Brownian motion parameter, however the higher values of thermophoresis parameter leads to an augmentation in the concentration of the nanoliquid for both situations ($n < 1$) and ($n > 1$). The influence of higher values of the concentration Biot number γ_1 and Lewis number Le on the concentration field spectacles a conflicting impact which is expressed in figs. 11(a), (b) and 12(a), (b). An increase in the values of concentration Biot number enhances the concentration of the Carreau liquid and corresponds to the thickness of boundary layer while it declines for the Lewis number. From the physical point of assessment the Lewis number is the inversely amount to the Brownian diffusion coefficient owing to which a magnification in the Lewis produces a decline in the diffusion coefficient, hence the nanoparticles concentration and its thickness of boundary layer declines. Additionally, figs. 13(a), (b) and 14(a), (b) are schemed to comprehend the legitimacy of our flow problem on temperature distribution and reveal a remarkable settlement of the bvp4c scheme with the homotopy analysis method (HAM).

Table 1 is prepared to see the convergence of different flow parameters on the local Nusselt number and Sherwood number for both shear thinning/shear thickening liquids. From table 1 it is noted that the rate of heat and mass transfer decline for increasing values of the Brownian motion parameter for both situations ($n < 1$) and ($n < 1$) while

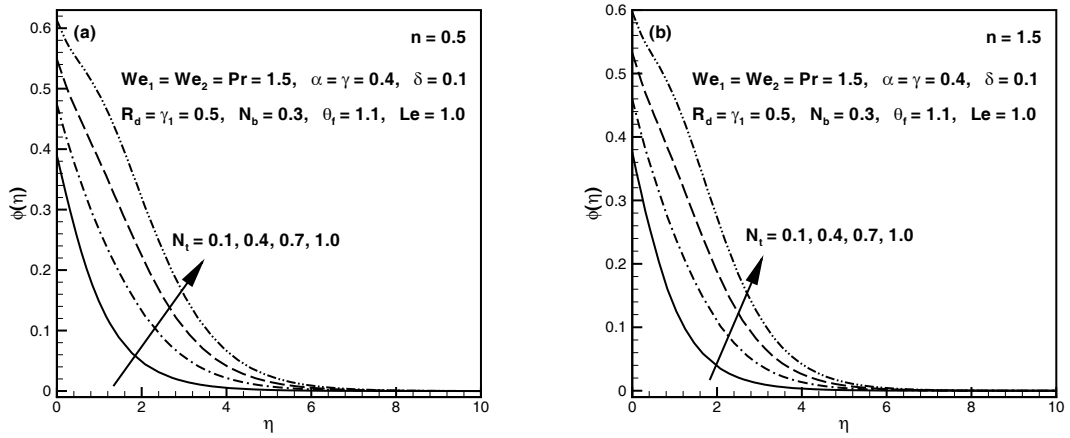

Fig. 10. Impact of thermophoresis parameter N_t on concentration field $\phi(\eta)$.

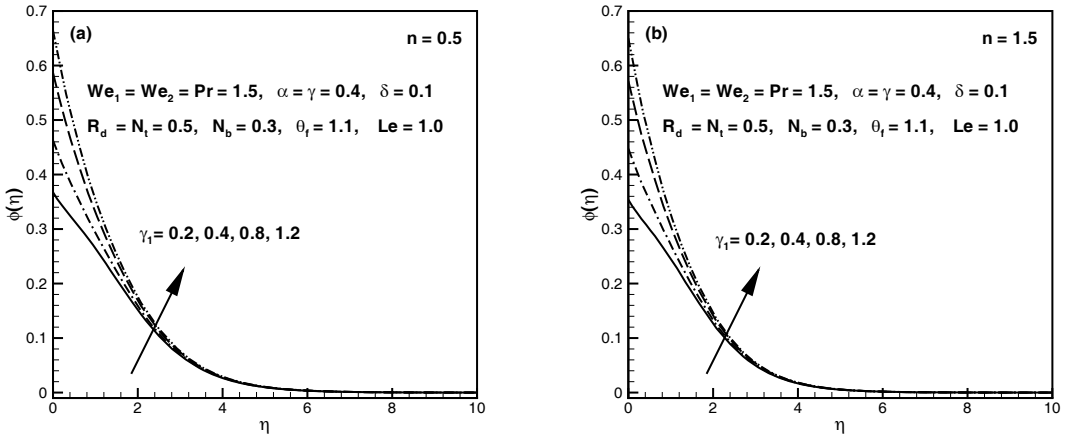

Fig. 11. Impact of concentration Biot number γ_1 on concentration field $\phi(\eta)$.

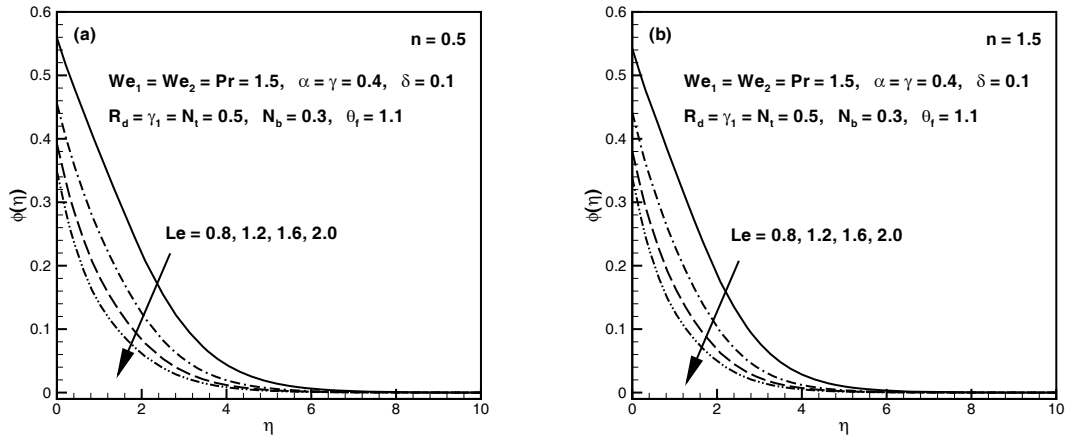

Fig. 12. Impact of Lewis number Le on concentration field $\phi(\eta)$.

the influence of amassed values of the concentration Biot number on the rate of heat transfer is quite reverse to the mass transfer rate. Moreover, table 2 is organized for the numerical values of the local Nusselt number and Sherwood number of two different schemes numerically (bvp4c) and analytically (HAM). In this table a tremendous agreement is established between both the techniques. Additionally, the validity of the numerical and analytical results are also presented by assessment with former related prose and remarked an excellent settlement in tables 3 and 4.

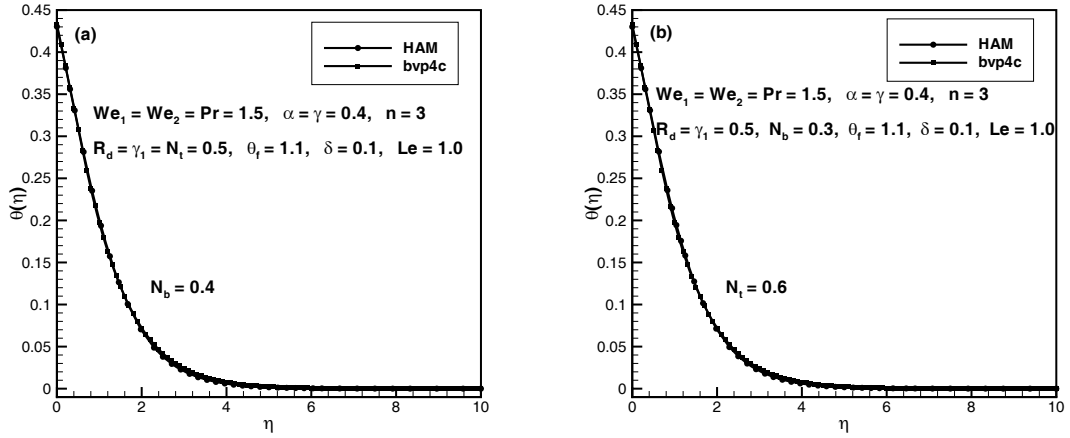

Fig. 13. Comparison between bvp4c and HAM of Brownian motion parameter N_b and thermophoresis parameter N_t on temperature field $\theta(\eta)$.

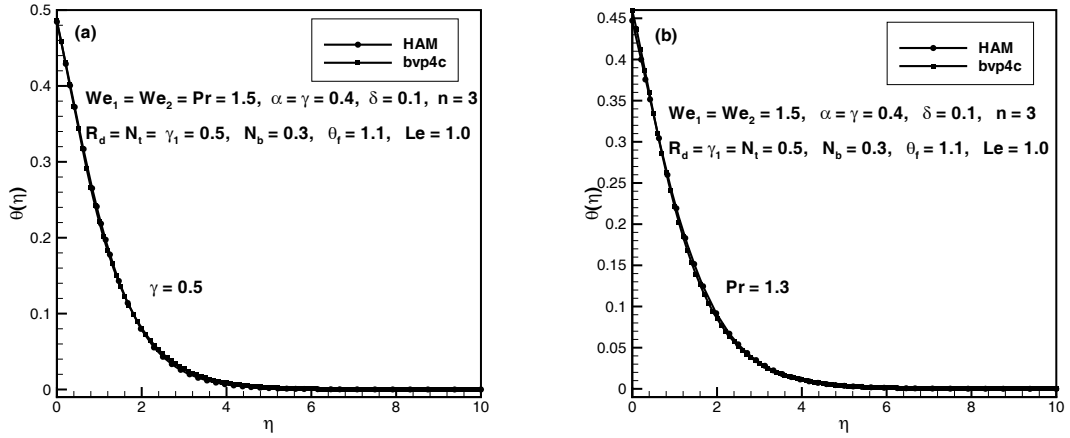

Fig. 14. Comparison between bvp4c and HAM of thermal Biot number γ and Prandtl number Pr on temperature field $\theta(\eta)$.

Table 1. Numerical values of local Nusselt number and local Sherwood number when $We_1 = We_2 = 1.5$, $\alpha = \gamma = 0.4$, $R_d = 0.5$, $\theta_f = 1.1$ are fixed.

N_t	N_b	δ	Pr	γ_1	Le	$\mathrm{Re}_x^{-\frac{1}{2}} Nu_x$		$\mathrm{Re}_x^{-\frac{1}{2}} Sh_x$	
						$n = 0.5$	$n = 1.5$	$n = 0.5$	$n = 1.5$
0.5	0.3	0.1	1.5	0.5	1.0	0.341960	0.355985	0.249964	0.257590
0.6						0.338322	0.352647	0.237525	0.245339
0.7						0.334630	0.349260	0.225651	0.233611
0.8						0.330883	0.345823	0.214344	0.222408
0.5	0.4					0.338260	0.352554	0.268821	0.275984
	0.5					0.334526	0.349089	0.280138	0.287025
	0.6					0.330758	0.345591	0.287685	0.294387
	0.3	0.0				0.366450	0.376012	0.239956	0.249322
		0.2				0.303074	0.327126	0.264898	0.268906
		0.3				0.213655	0.277479	0.296008	0.287032
		0.1	1.2			0.318472	0.334126	0.227834	0.235484
			1.4			0.334979	0.349493	0.243130	0.250807
			1.6			0.348263	0.361847	0.256325	0.263875
			1.5	0.7		0.340017	0.354120	0.307357	0.317713
				0.9		0.338491	0.352645	0.351684	0.365050
				1.0		0.337845	0.352018	0.370532	0.385135
				0.5	0.8	0.342023	0.356046	0.220321	0.228760
					1.1	0.342000	0.356019	0.261808	0.269075
					1.3	0.342155	0.356154	0.281407	0.288046

Table 2. Numerical values of the local Nusselt number and local Sherwood number for two different techniques when $We_1 = We_2 = R_d = 0.5$, $\alpha = 0.4$, $\theta_f = 1.1$, $\delta = 0.1$ and $n = 3$ are fixed.

N_t	N_b	Pr	γ	γ_1	Le	$\mathrm{Re}_x^{-\frac{1}{2}} Nu_x$		$\mathrm{Re}_x^{-\frac{1}{2}} Sh_x$	
						bvp4c	HAM	bvp4c	HAM
0.2	0.3	1.5	0.3	0.3	1.0	0.305948	0.305959	0.209633	0.209637
0.3						0.304038	0.304044	0.201220	0.201222
0.4						0.302094	0.302103	0.193054	0.193052
0.5						0.300115	0.300122	0.185130	0.185111
0.2	0.1					0.309066	0.309069	0.173196	0.173163
	0.2					0.307515	0.307514	0.200523	0.200517
	0.4					0.304366	0.304366	0.214189	0.214189
	0.3	1.4				0.301094	0.301095	0.206679	0.206681
		1.7				0.314283	0.314288	0.214797	0.214788
		2.0				0.324258	0.324252	0.221128	0.221090
		1.5	0.1			0.130296	0.130298	0.219452	0.219449
			0.2			0.229213	0.229214	0.213837	0.213841
			0.4			0.366754	0.366757	0.206396	0.206392
			0.3	0.2		0.307140	0.307149	0.151935	0.151942
				0.4		0.304926	0.304945	0.258768	0.258776
				0.5		0.304040	0.304052	0.301115	0.301111
				0.3	0.7	0.305733	0.305746	0.190679	0.190708
					0.8	0.305794	0.305800	0.198174	0.198188
					1.2	0.218066	0.218049	0.306115	0.306117

Table 3. An assessment table of $-f''(0)$ in limiting sense when $We_1 = We_2 = 0$ and $n = 3$ are fixed.

α	$-f''(0)$			
	Wang [34]	Liu and Anderson [35]	Present (bvp4c)	Present (HAM)
0.0	1	1	1	1
0.25	1.048813	1.048813	1.0488130	1.0488131
0.50	1.093097	1.093096	1.0930954	1.0930943
0.75	1.134485	1.134486	1.1344854	1.1344858
1.0	1.173720	1.173721	1.1737199	1.1737201

Table 4. An assessment table of $-g''(0)$ in limiting sense when $We_1 = We_2 = 0$ and $n = 3$ are fixed.

α	$-g''(0)$			
	Wang [34]	Liu and Anderson [35]	Present (bvp4c)	Present (HAM)
0.0	0	0	0	0
0.25	0.194564	0.194565	0.1945652	0.1945617
0.50	0.465205	0.465206	0.4652058	0.4652047
0.75	0.794622	0.794619	0.7946180	0.7946184
1.0	1.173720	1.173721	1.1737199	1.1737201

6 Main results

The current exploration inspects the impact of the nonlinear thermal radiation on 3D flow of the Carreau nanofluid over a bidirectional stretched surface. Effects of heat source/sink with convective heat and mass transfer mechanisms are also considered. The bvp4c technique is engaged to solve the Carreau nanofluid problem. Important outcomes of the modeled problem are as follows:

– Both the temperature and concentration profile were augmenting functions of thermal and concentration Biot numbers (γ, γ_1), respectively.
– Opposite behavior was noticed for amassed values of heat generation and absorption parameters on the temperature distribution for both shear thinning/thickening cases.

– Increase in the values of thermal radiation parameter R_d intensifies the temperature and its allied thickness of boundary layer in both circumstances.
– Enhancing the values of thermophoresis parameter N_t augmented both the temperature and nanoparticle concentration field on the other hand the impact of Brownian motion parameter N_b on the temperature profile was quite differing to the concentration of the Carreau nanofluid for $(n < 1)$ and $(n > 1)$.

References

1. S.U.S. Choi, ASME Int. Mech. Eng. **66**, 99 (1995).
2. J. Buongiorno's, ASME J. Heat Transf. **128**, 240 (2006).
3. R. Ellahi, M. Hassan, A. Zeeshan, Int. J. Heat Mass Transfer **81**, 449 (2015).
4. B. Mahanthesh, B.J. Gireesha, R.S.R. Gorla, F.M. Abbasi, S.A. Shehzad, J. Magn. & Magn. Mater. **417**, 189 (2016).
5. M. Khan, W.A. Khan, AIP Adv. **6**, 02521 (2016).
6. T. Hayat, M.I. Khan, M. Waqas, A. Alsaedi, M. Farooq, Comput. Methods Appl. Mech. Eng. **315**, 1011 (2017).
7. W.A. Khan, M. Irfan, M. Khan, A.S. Alshomrani, A.K. Alzahrani, M.S. Alghamdi, J. Mol. Liq. **234**, 201 (2017).
8. R.U. Haq, S.N. Kazmi, T. Mekkaoui, Int. J. Heat Mass Transfer **112**, 972 (2017).
9. T. Hayat, M.I. Khan, M. Waqas, A. Alsaedi, Results Phys. **7**, 256 (2017).
10. M. Khan, M. Irfan, W.A. Khan, A.S. Alshomrani, Results Phys. **7**, 2692 (2017).
11. P. Besthapu, R.U. Haq, S. Bandari, Q.M. Al-Mdallal, J. Taiwan Inst. Chem. Eng. **71**, 307 (2017).
12. M. Khan, M. Irfan, W.A. Khan, Int. J. Mech. Sci. **130**, 375 (2017).
13. F.A. Soomro, R.U. Haq, Z.H. Khan, Q. Zhang, Chin. J. Phys. **55**, 1561 (2017).
14. M. Khan, M. Irfan, W.A. Khan, Int. J. Hydrog. Energy **42**, 22054 (2017).
15. I. Rashid, R.U. Haq, Q.M. Al-Mdallal, Physica E **89**, 33 (2017).
16. T. Hayat, M. Rashid, M. Imtiaz, A. Alsaedi, AIP Adv. **6**, 067169 (2015).
17. F. Shahzad, R.U. Haq, Q.M. Al-Mdallal, J. Mol. Liq. **224**, 322 (2016).
18. M. Atlas, R.U. Haq, T. Mekkaoui, J. Mol. Liq. **223**, 289 (2016).
19. R.U. Haq, F. Shahzad, Q.M. Al-Mdallal, Results Phys. **7**, 57 (2016).
20. T. Hayat, M. Rashid, M. Imtiaz, A. Alsaedi, J. Mol. Liq. **225**, 482 (2017).
21. M.S. Anwar, A. Rasheed, Chin. J. Phys. **55**, 1690 (2017).
22. P.J. Carreau, Trans. Soc. Rheol. **16**, 99 (1972).
23. N.S. Akbar, S. Nadeem, Ain Shams Eng. J. **5**, 1307 (2014).
24. T. Hayat, M. Waqas, S.A. Shehzad, A. Alsaedi, Pramana J. Phys. **86**, 3 (2016).
25. A. Aziz, Commun. Nonlinear Sci. Numer. Simul. **14**, 1064 (2009).
26. T. Hayat, Y. Saeed, A. Alsaedi, S. Asad, PLoS ONE **10**, e0133831 (2015).
27. T. Hayat, M. Waqas, S.A. Shehzad, A. Alsaedi, J. Mol. Liq. **215**, 704 (2016).
28. M. Khan, M. Irfan, W.A. Khan, L. Ahmad, Results Phys. **7**, 1899 (2017).
29. M. Irfan, M. Khan, W.A. Khan, Results Phys. **7**, 3315 (2017).
30. M. Khan, L. Ahmad, W.A. Khan, A.S. Alshomrani, J. Mol. Liq. **224**, 1016 (2016).
31. T. Hayat, M. Rashid, A. Alsaedi, Results Phys. **7**, 3107 (2017).
32. M. Waqas, M.I. Khan, T. Hayat, A. Alsaedi, Results Phys. **7**, 2489 (2017).
33. T. Hayat, M.I. Khan, M. Waqas, A. Alsaedi, Results Phys. **7**, 2197 (2017).
34. C.Y. Wang, Phys. Fluids **27**, 1915 (1984).
35. I.C. Liu, H.I. Anderson, Int. J. Heat Mass Transfer **51**, 4018 (2008).